The 9th European Congress on Computational Methods in Applied Sciences and Engineering
ECCOMAS Congress 2024
3–7 June 2024, Lisboa, Portugal

IMPLEMENTATION OF RHT MATERIAL MODEL FOR BOULDERS AND CONCRETE IN MULTI-LAYERED COMPOSITE TARGET UNDER PROJECTILE IMPACT

Shashwat Kapoor[1], **Sonalisa Ray**[2]

[1] Civil Engineering Department
Indian Institute of Technology Roorkee, India
e-mail: shashwat_k@ce.iitr.ac.in

[2] Civil Engineering Department
Indian Institute of Technology Roorkee, India
e-mail: sonalisa.ray@ce.iitr.ac.in

Key words: High-velocity projectile impact, Multi-layered composite, User-subroutine (VUMAT), Mesoscale modelling, Failure mechanism

Summary. Innovative solutions are crucial to enhance protection against ballistic impacts on military structures, especially as conventional materials like homogeneous concrete may prove inadequate. Exploring functionally graded layered composite structures with diverse material properties becomes imperative. Hence, a computational framework is developed to comprehensively analyze these systems, with validation conducted for triple-layered targets. The Riedel, Hiermaier, and Thoma (RHT) material model is implemented to model boulders and concrete using a user-defined subroutine interface (VUMAT). The study involves a detailed assessment of the complete energy balance and absorbed energy by the multi-layered composite, which incorporates reinforced concrete, boulder-mixed soil, hyper-elastic rubber, and hot-rolled steel plates. This comprehensive approach, utilizing finite element analysis, focuses on investigating the influence of projectile impact on the resultant failure mechanisms of the multi-layered composite target. The research findings present potential applications in the design of military protective structures.

1 INTRODUCTION

Brittle materials, such as rock and concrete, play an important role in civil and military engineering constructions. These materials often encounter impact loads in practical engineering scenarios such as projectile impacts, tunneling, and mining. The dynamic damage process in these materials is highly complex due to numerous pre-existing micro-cracks. Existing material models, which primarily rely on empirical or semi-empirical formulas, cannot capture the complexity of this dynamic damage. Since the principles of brittle fracture are fundamentally based on physical laws, they are best described through a constitutive model. Consequently, it is essential to investigate the evolution of damage in brittle materials under impact loads using constitutive relationships.

Previous experimental research has revealed varying mechanical responses of brittle materials under tensile and compressive loads. Furthermore, dynamic mechanical behaviors of brittle

materials differ significantly from those observed under quasi-static conditions [1]. One notable mechanical characteristic is the increased material strength with strain rate. Over recent years, several blasting damage models, such as the Holmquist-Johnson-Cook (HJC), Taylor-Chen-Kuszmaul (TCK), Johnson-Holmquist (JH-2), and Riedel-Hiermaier-Thoma (RHT) models, have been developed and implemented to account for the strain rate effect and damage evolution mechanisms of brittle materials. However, these models have needed to exhibit more accurate descriptions of the mechanical properties of brittle material. These models have been modified to address dynamic tension-compression asymmetry, including efforts by Polanco-Loria et al.[2] and Kong et al. [3]. Li and Shi [4] have proposed a dynamic material model considering high strain rates and pressures, while Xie et al. [5] have incorporated strain rate effects into the RHT model. Despite these advancements, inconsistencies between model predictions and experimental data in high-strain rate areas have persisted. Tu and Lu [6] have further improved the RHT model but have lacked corresponding to laboratory mechanical experiments to validate the modifications.

In addition, various researchers have investigated combinations of different materials, such as composite-metal hybrid structures subjected to impact loading. Ramadhan et al. [7] have conducted an experimental and numerical study on a sandwich structure consisting of Kevlar-29 fiber/epoxy resin with 6061-T6 aluminum plates, finding that the novel sandwich structures exhibit good energy absorption efficiency when subjected to projectile impact. Kapoor et al. [8, 9] and Pattajoshi et al. [10, 11, 12] have proposed multi-layer composite structures and investigated their dynamic characteristics under projectile impact loads, showing that these multi-layer composite targets demonstrate improved resistance to penetration and experience less damage compared to reinforced concrete monolayer structures. Moreover, Majzoobi et al. [13] have investigated the ballistic limit of bi-metal 2/1 functionally graded metal laminates (FMLs) composed of aluminum and titanium.

In the present study, a computational approach has been developed to investigate multi-layered composite targets subjected to a deformable projectile, in which the soil layer acts as a camouflage layer, boulders-mixed soil as an anti-penetration layer, a steel plate as an energy absorption layer, and EPDM rubber as a shock absorption layer. The RHT model has been proposed to enhance its ability to predict the tensile behaviors of brittle materials like boulders and concrete under projectile impact. The RHT model has been implemented using the VUMAT subroutine in ABAQUS/EXPLICIT, and its effectiveness has been demonstrated through single-element tests. Subsequently, the RHT model has been validated by comparing numerical predictions with experimental results.

2 CONSITUTIVE MODELLING

This section provides a brief description of the various material models used to describe the behavior of each layer in a composite target when subjected to projectile impact, as listed in Table 1. The detailed description of the Riedel-Hiermaier-Thoma material model is described in Section 2.1.

2.1 Riedel-Hiermaier-Thoma Model

The Riedel-Hiermaier-Thoma (RHT) model [14, 15] for brittle materials like concrete and boulders considers strain hardening, strain rate hardening, strain softening, pressure hardening,

Table 1: Material models used in multi-layered composite target

S. No.	Materials	Equation of State	Strength Model	Failure Model
1.	Sandy soil (Layer-6)	Linear	Mohr - Coulomb	-
2.	Boulders (Layer-5)	Polynomial	RHT	RHT
3.	MS Plate (Layer-4)	Shock	Johnson Cook	Johnson Cook
4.	Concrete-35MPa (Layer-3 & Layer-1)	Polynomial	RHT	RHT
5.	Reinforcement (Layer-3 & Layer-1)	Shock	Johnson Cook	Johnson Cook
6.	Ballistic Rubber (Layer-2)	Hyper-elastic	Ogden - 3rd Order	-
7.	Projectile	Shock	Johnson Cook	Johnson Cook

and third stress invariant dependence. The RHT model considers three pressure-dependent surfaces: elastic limit, failure, and residual strength surfaces. For a stress state, the generalized failure surface for the RHT model is given by:

$$f(P, \sigma_{eq}, \theta, \dot{\varepsilon}) = \sigma_{eq} - Y_{TXC}(P) \times F_{CAP}(P) \times R_3(\theta) \times F_{RATE}(\dot{\varepsilon}) \tag{1}$$

where; $Y_{TXC}(P)$ represents the compressive meridian and is given as follows:

$$Y_{TXC} = f_c \cdot A \left(\frac{P}{f_c} - P^*_{spall} \cdot F_{rate} \right)^N \tag{2}$$

where f_c, P, P_{spall} represents cylinder strength, pressure, and normalized hydrodynamic tensile limit, respectively. $R_3(\theta)$ represents the lode angle as follows:

$$R_3 = \frac{r}{r_c} = \frac{2(1-Q_2^2)cos\theta + (2Q_2 - 1)\sqrt{4(1-Q_2^2)cos^2\theta - 4Q_2}}{4(1-Q_2^2)cos^2\theta + (1-2Q_2)^2} \tag{3}$$

where,

$$\cos(3\theta) = \frac{3\sqrt{3}J_3}{2^{\frac{3}{2}}\sqrt{J_2}} \tag{4}$$

$$Q_2 = Q_{2,0} + BQ.P^*; 0.51 < Q_2 < 1 \tag{5}$$

$F_{RATE}(\dot{\varepsilon})$ represents dynamic increase factor as follows:

$$\begin{aligned} F_{rate}(\dot{\varepsilon}) = DIF &= \left[\frac{\dot{\varepsilon}}{\dot{\varepsilon}_0} \right]^{\alpha} \; for\ compression\ (P^* > \frac{1}{3}) \\ &= \left[\frac{\dot{\varepsilon}}{\dot{\varepsilon}_0} \right]^{\delta} \; for\ tension\ (P^* < \frac{1}{3}) \end{aligned} \tag{6}$$

where $\dot{\varepsilon}$, $\dot{\varepsilon}_0$, α and, δ represent strain rate, reference strain rate, compressive strain rate exponent, and tensile strain rate exponent, respectively. The elastic limit surface of RHT model is given as follows:

$$Y_{elastic} = Y_{failure} \times F_{elastic} \times F_{cap} \tag{7}$$

where $F_{elastic}$ represents inelastic stresses occurring under compressive loading at 30% and under tension at 50-80% of maximum loading capacity and, F_{cap} represent consistency among inelastic volumetric and deviatoric stresses. Strain hardening is represented in the model by defining an elastic limit surface and a "hardening" slope as follows:

$$Y^* = Y_{elastic} + \frac{\epsilon_{pl}}{\epsilon_{pl(pre-softening)}} (Y_{fail} - Y_{elastic}) \tag{8}$$

where,

$$\epsilon_{pl(pre-softening)} = \frac{Y_{fail} - Y_{el}}{3G} \times \left(\frac{G_{elastic}}{G_{elastic} - G_{plastic}} \right) \tag{9}$$

And strain softening of the RHT model is represented as follows:

$$Y_{fractured} = (1 - D)Y_{failure} + DY_{residual} \tag{10}$$

Where $Y_{residual}$ represents the residual surface of the RHT model as follows:

$$Y_{residual} = \min[B(P^*)^M, Y_{TXC} \times SF_{MAX}] \tag{11}$$

Where $Y_{TXC} \times SF_{MAX}$ limits the maximum residual shear strength (for completely damaged material) to be a fraction (SF_{MAX}) of the current fracture strength. Damage is assumed to accumulate due to inelastic deviatoric straining as follows:

$$D = \sum \frac{\Delta \epsilon_{pl}}{\epsilon_p^{failure}} \tag{12}$$

$$\epsilon_p^{failure} = D_1 (P^* - P^*_{spall})^{D_2}$$

where D_1 and D_2 are material constants that describe the effective strain to fracture as a function of pressure.

3 NUMERICAL MODELLING

This section presents the methodology for analyzing the multi-layered composite target subjected to deformable projectile impact. The target configuration consists of a multi-layered 600 $mm \times 600$ $mm \times 430$ mm structure subjected to the impact of a 329 g ogive-shaped projectile [16] with a diameter of 25.3 mm and a length of 151.9 mm at a normal incident velocity of 330 m/s, as shown in Figure 1. The multi-layered composite target consists of six different layers: the top layer, a sandy soil layer of thickness 50 mm, acts as a camouflage layer; a boulders-mixed soil layer of thickness 100 mm, with boulders having an unconfined compressive strength of 120 MPa, acts as an anti-penetration layer; a steel plate of thickness 10 mm acts as an energy absorption layer; EPDM rubber of thickness 50 mm acts as a shock absorption layer; and RCC layer (M35 grade) of thickness 120 mm acts as base slab of multi-layered composite target, as depicted in Figure 2.

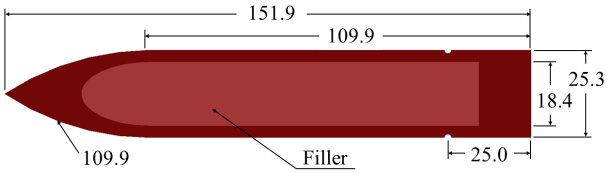

Figure 1: Geometry of projectile (all dimensions are in mm).

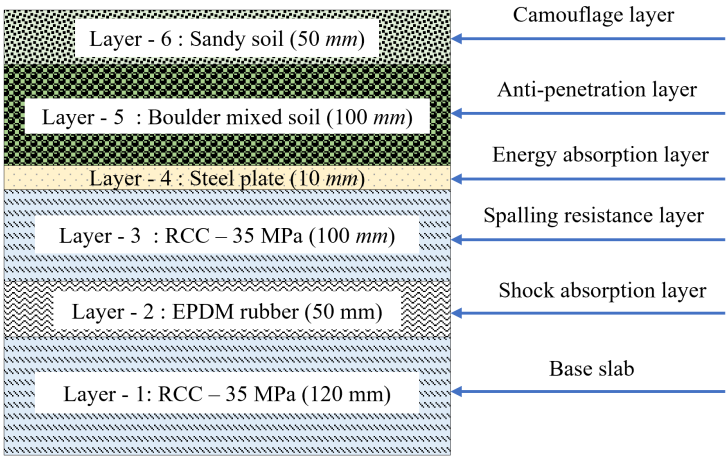

Figure 2: Configuration of multi-layered composite target

Multi-layered targets and deformable projectiles are modeled using 3-D continuum brick elements with reduced integration (C3D8R) and 10-node modified quadratic tetrahedron elements (C3D10M), respectively. The interaction between the projectile and the target is assigned using surface-to-surface interaction, considering the projectile as the master surface and the impact regions of the target as the slave surface. The interaction between the contacting surfaces of the layers is also assigned using surface-to-surface interaction, with the higher stiffness layer as the master surface and the other layers as the slave surface. Additionally, a tie constraint is used as an interaction between randomly distributed boulders and the soil matrix. A friction coefficient of 0.3 is considered between the projectile and the target and between the interfaces of the individual layers of the multi-layered target [17]. Fixed boundary conditions are applied to the outer faces of the multi-layered targets, while an embedded region constraint is used to constrain reinforcement bars, each having a diameter of 10 mm and spaced at intervals of 100 mm within the concrete.

Table 2: Material model shear parameters for EPDM elastomer [18].

i	Shear modulus (μ_i)	Constant(α_i)
1	0.99	3.36
2	0.06	9.76
3	0.07	-4.61

The RHT material model was used to model M35 concrete. The material parameters for the concrete layer were obtained from the study by Tu et al. [14]. The behavior of the reinforcement

Table 3: RHT material model parameters of brittle materials.

Parameters	Symbols	Concrete [14]	Boulders [19]
Density	ρ (kg/m^3)	2500	2700
Young's modulus	E (MPa)	29580	54772
Compressive strength	f_c (MPa)	35	120
Tensile strength	f_t/f_c	0.1	0.1
Shear strength	f_s/f_c	0.18	0.2
Intact failure surface constant	A	1.6	1.6
Intact failure surface exponent	N	0.61	0.61
Tens./Comp. meridian ratio	Q	0.6805	0.6805
Brittle to ductile transition	BQ	0.0105	0.0105
$G_{elastic}/(G_{elastic} - G_{plastic})$	-	2	2
Elastic strength/ft	-	0.7	0.7
Elastic strength/fc	-	0.53	0.53
Fractured strength constant	B	1.6	1.68
Fractured strength exponent	M	0.61	0.39
Compressive strain-rate exponent	α	0.032	0.02
Tensile strain rate exponent	δ	0.036	0.025

Table 4: Johnson-Cook material model parameters of ductile materials.

Parameters	Symbols	Reinforcement bars [20]	Weldox 460 E steel plate [21]	Projectile casing [22]
Material density	ρ (kg/m^3)	7850	7850	7860
Modulus of elasticity	E (GPa)	201	203	210
Poisson's ratio	μ	0.30	0.33	0.25
Yield stress constant	A (MPa)	500	490	1539
Strain hardening constant	B (MPa)	807	807	477
Strain hardening exponent	n	0.73	0.73	0.18
Viscous effect	C	0.0114	0.0114	0.012
Thermal softening constant	m	0.94	0.94	1
Reference strain rate	$\dot{\epsilon}_0$	0.0005	0.0005	0.001
Fracture strain constants	D_1	0.0705	0.0705	0.15
	D_2	1.732	1.732	0.72
	D_3	-0.54	-0.54	1.66
	D_4	-0.015	-0.015	0
	D_5	0	0	0

bars was incorporated using the JC model, and the material parameters were adopted from Rajput et al. [20]. The material model parameters for the Weldox 460 E steel plate were obtained from Børvik et al. [21]. The EPDM elastomer layer was modeled using the Ogden model, and the material parameters were obtained from Feichter et al. [18] as reported in Table 2. The Mohr-Coulomb model was used to model the sandy soil layer. Additionally, the boulders were modeled using the RHT model, and the material parameters were obtained from Guo et al. [19]. Table 3 lists the brittle materials incorporating the RHT model parameters, while Table 4 lists the ductile materials incorporating the JC model parameters. These constitutive models and their respective material parameters comprehensively represented the material behavior within the multi-layered target system.

4 NUMERICAL VALIDATION

4.1 Single element analysis

The numerical validation of the RHT material model has been carried out using the brick element with reduced integration (C3D8R) of size 1 mm × 1 mm × 1 mm under uniaxial compression and tension loading conditions. The displacement constraint boundary condition has been applied on the bottom face of the single element to avoid rigid-body motion under both loading conditions, as shown in Figure 3(a).

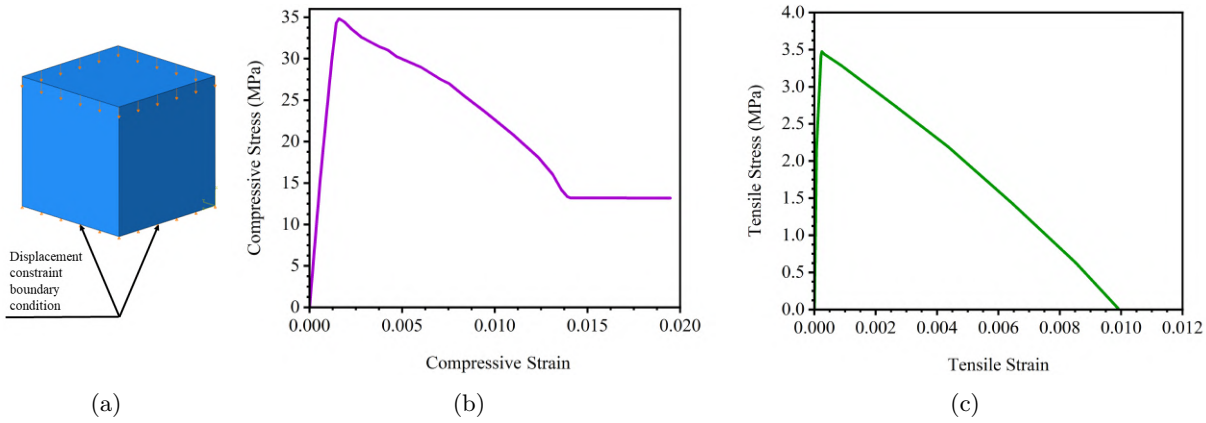

Figure 3: (a) Single element analysis.; (b) Compressive stress-strain curve.; (c) Tensile stress-strain curve.

Figure 3(b) represents the simulated stress-strain relationship under uniaxial compressive loading, which correctly simulates the unconfined compressive strength of the concrete cube. However, the default RHT model predicted larger softening behavior and became perfectly plastic after reaching a softening point at 14 MPa. Similarly, Figure 3(c) represents the simulated stress-strain relationship under uniaxial tensile loading, which overestimates the tensile strength of the concrete and consequently shows the decaying softening of concrete material under tension.

4.2 Single layer target

In this analysis phase, the numerical validation of experimental results conducted by Hanchak et al. [23] has been performed. They have conducted impact tests on reinforced concrete (RCC) slabs of size 610 mm × 610 mm × 178 mm with 500 g ogive-shaped projectile measuring 143.7 mm in length and 25.4 mm in diameter as shown in Figure 4. For the RCC slab with an unconfined compressive strength of 48 MPa, the projectile has been launched at striking velocities ranging from 301-1058 m/s. Similarly, for the RCC slab with an unconfined compressive strength of 140 MPa, the striking velocities have ranged from 376-998 m/s.

For the numerical study, the RHT model was employed for the constitutive modeling of concrete with compressive strengths of 48 MPa and 140 MPa. The concrete slab was discretized using 8-noded linear 3D brick elements (C3D8R), and the reinforcement bars were meshed using 2-noded truss elements (T3D2). Figure 5 compares the residual and impact velocities from the current simulations and the experimental data. This comparison incorporates RCC slabs with

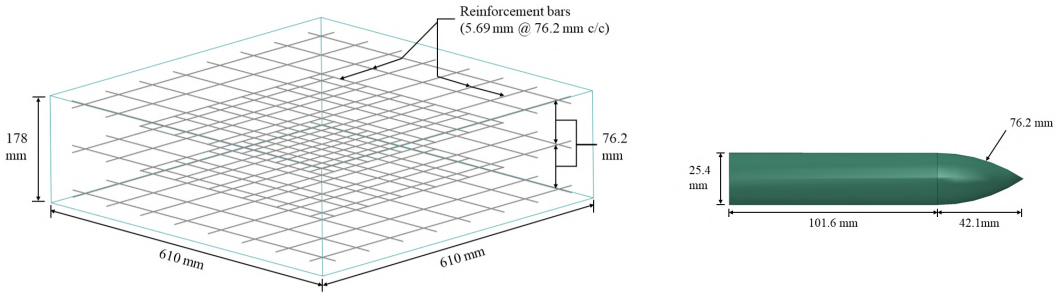

(a) (b)

Figure 4: Geometry of (a) RCC Slab; (b) Projectile

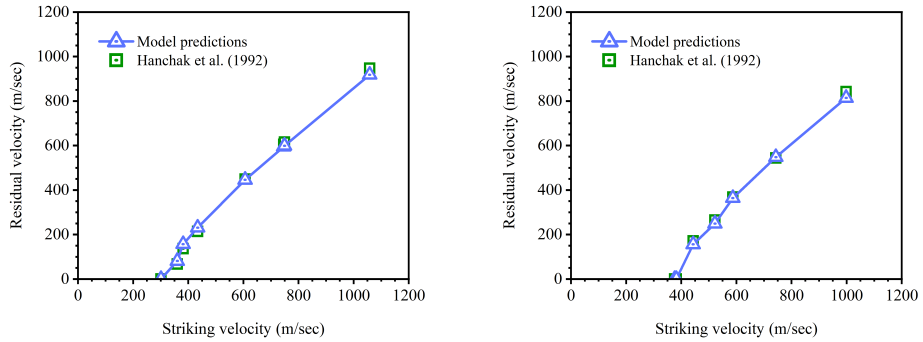

(a) (b)

Figure 5: Validation of FE simulation results with experimental data of (a) M48; (b) M140; RCC slab.

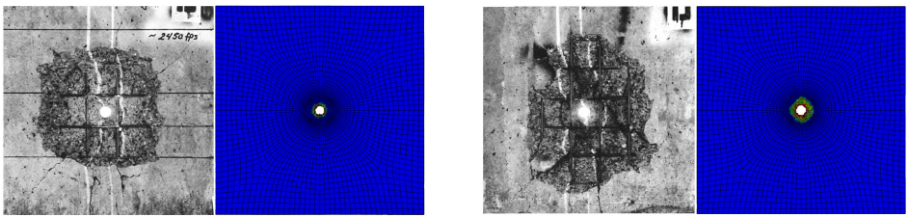

(a) 48 MPa front crater and damage (b) 48 MPa rear crater and damage

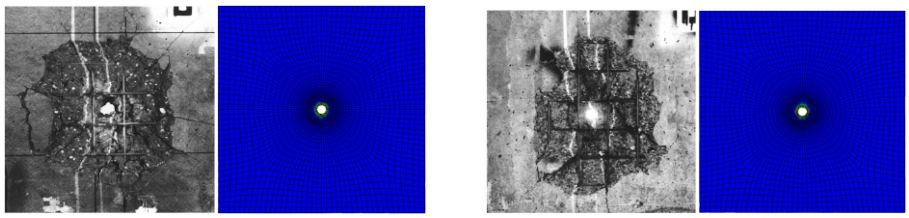

(c) 140 MPa front crater and damage (d) 140 MPa rear crater and damage

Figure 6: Experimental [23] and numerical simulation comparison of front and rear damage area.

compressive strengths of 48 MPa and 140 MPa. However, it was observed that the crater diameter estimated in this study is underestimated due to the overestimation of the tensile strength of the RHT model, as depicted in Figure 6.

5 RESULTS AND DISCUSSION

5.1 Ballistic performance

The longitudinal deformed section of the multi-layered target subjected to an ogive-shaped projectile impact has been presented in Figure 7(a). The depth of penetration (DOP) of the projectile was found to be 236 mm. Furthermore, once the penetration has been completed, the projectile exhibited a ricochet phenomenon [24], altering its trajectory angle upon impacting the surface within the multi-layered targets.

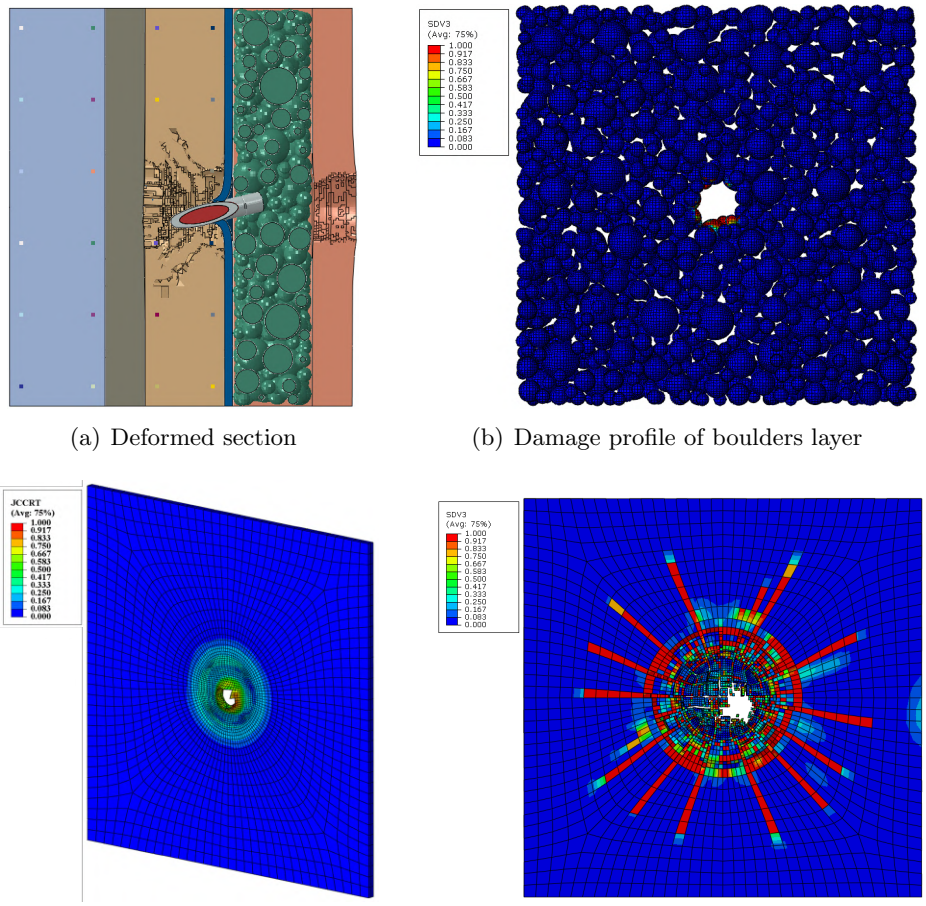

(a) Deformed section

(b) Damage profile of boulders layer

(c) Damage profile of steel layer

(d) Damage profile of RCC layer

Figure 7: Numerical simulation results of the multi-layered composite target.

When the projectile interacted with the sandy soil layer, it led to minimal kinetic energy absorption since it only acted as a camouflage layer to blend with the environment seamlessly. However, when the projectile encountered the boulders layer, a sudden increase in kinetic energy

absorption was observed due to the ricochet phenomenon, which deviated the projectile from its initial line of trajectory, as the boulders mixed soil acted as an anti-penetration layer. Subsequently, the EPDM rubber layer, being highly deformable, has led to minimal kinetic energy absorption since it acted as a shock absorption layer to mitigate the stress wave propagation to the base slab of the military bunker.

5.2 Damage characteristics

The dynamic fracture behavior of each layer in the multi-layered composite target has been essential for determining the overall performance and protective capabilities of the structure under projectile impact. Each layer has displayed distinct damage characteristics and has contributed to the overall resistance against projectile impact.

The projectile interacted with the sandy soil layer in the initial impact stage, leading to material erosion and ductile hole enlargement. The impact impulse has exceeded the dynamic strength at the periphery of the soil material, resulting in its outward displacement and the formation of a crater considerably larger than the diameter of the projectile. Upon encountering the boulder-mixed soil layer, the boulders have experienced highly localized brittle damage, with fragmentation failure confined to the specific boulder that has been in contact with the projectile, as shown in Figure 7(b). When the projectile interacted with the steel plate layer, intense radial and circumferential tensile stresses emerged near the tip of the projectile following the passage of the shock wave, leading to highly localized ductile damage, as shown in Figure 7(c). Upon impacting the intermediate RCC layer, the formation of craters, accompanied by the removal of fragments from front and rear surface and the generation of high-pressure shock waves, has led to spalling and scabbing damage in the RCC layer, as shown in Figure 7(d).

6 CONCLUSIONS

The present study has investigated the impact of an ogive-shaped projectile on a multi-layered composite target with dimensions of 600 $mm \times 600\ mm \times 430\ mm$. The study has extensively explored the ballistic performance and damage characteristics of the individual layers of the multi-layered composite target. The key findings can be summarized as follows:

- The proposed multi-layered composite target has shown improved penetration resistance and sustained less damage than the monolayer-reinforced concrete target.
- The boulder-mixed soil layer has demonstrated its capability to withstand impact loading. The interaction between the projectile and randomly distributed boulders has caused the projectile to ricochet upon impact.
- These findings suggest that incorporating multi-layered composites in designing and constructing military bunkers is effective and promising potential savings in military infrastructure.

REFERENCES

[1] P. Liu, K. Liu, Q.-B. Zhang, Experimental characterisation of mechanical behaviour of concrete-like materials under multiaxial confinement and high strain rate, Construction and Building Materials 258 (2020) 119638.

[2] M. Polanco-Loria, O. Hopperstad, T. Børvik, T. Berstad, Numerical predictions of ballistic limits for concrete slabs using a modified version of the hjc concrete model, International Journal of Impact Engineering 35 (5) (2008) 290–303.

[3] X. Kong, Q. Fang, H. Wu, Y. Peng, Numerical predictions of cratering and scabbing in concrete slabs subjected to projectile impact using a modified version of hjc material model, International Journal of Impact Engineering 95 (2016) 61–71.

[4] H. Y. Li, G. Y. Shi, A dynamic material model for rock materials under conditions of high confining pressures and high strain rates, International Journal of Impact Engineering 89 (2016) 38–48.

[5] L. X. Xie, W. B. Lu, Q. Zhang, Q. Jiang, M. Chen, J. Zhao, Analysis of damage mechanisms and optimization of cut blasting design under high in-situ stresses, Tunnelling and Underground Space Technology 66 (2017) 19–33.

[6] Z. Tu, Y. Lu, Modifications of rht material model for improved numerical simulation of dynamic response of concrete, International Journal of Impact Engineering 37 (10) (2010) 1072–1082.

[7] A. Ramadhan, A. A. Talib, A. M. Rafie, R. Zahari, High velocity impact response of kevlar-29/epoxy and 6061-t6 aluminum laminated panels, Materials & Design 43 (2013) 307–321.

[8] S. Kapoor, S. Ray, J. P. Sahoo, Y. K. Joshi, Optimization of multi-layered composites against ballistic impact: A mesoscale approach, Composite Structures 338 (2024) 118097.

[9] S. Kapoor, S. Ray, Optimization of multi-layered composite structures against impact loading, in: International Symposium on Plasticity and Impact Mechanics, Springer, 2022, pp. 269–284.

[10] S. Pattajoshi, S. Ray, Dynamic fracture behavior of layered composite under high strain rate loading, in: International Symposium on Plasticity and Impact Mechanics, Springer, 2022, pp. 305–322.

[11] S. Pattajoshi, S. Ray, Y. K. Joshi, Dynamic behaviour of multi-layer composite against single and multiple projectile impact loading, Theoretical and Applied Fracture Mechanics 129 (2024) 104189.

[12] J. C. Kishen, A. Ramaswamy, S. Ray, et al., Computational modeling of dynamic fracture of layered composite under various strain-rate loading.

[13] G. Majzoobi, H. Morshedi, K. Farhadi, The effect of aluminum and titanium sequence on ballistic limit of bi-metal 2/1 fmls, Thin-Walled Structures 122 (2018) 1–7.

[14] Z. Tu, Y. Lu, Evaluation of typical concrete material models used in hydrocodes for high dynamic response simulations, International Journal of Impact Engineering 36 (1) (2009) 132–146.

[15] W. Riedel, K. Thoma, S. Hiermaier, E. Schmolinske, Penetration of reinforced concrete by beta-b-500 numerical analysis using a new macroscopic concrete model for hydrocodes, in: Proceedings of the 9th International Symposium on the Effects of Munitions with Structures, Vol. 315, Berlin-Strausberg Germany, 1999.

[16] W. Wan, J. Yang, G. Xu, Y. Liu, Determination and evaluation of holmquist-johnson-cook constitutive model parameters for ultra-high-performance concrete with steel fibers, International Journal of Impact Engineering 156 (2021) 103966.

[17] C. S. Meyer, I. G. Catugas, J. W. Gillespie Jr, B. Z. G. Haque, Investigation of normal, lateral, and oblique impact of microscale projectiles into unidirectional glass/epoxy composites, Defence Technology 18 (11) (2022) 1960–1978.

[18] C. Feichter, Z. Major, R. Lang, Deformation analysis of notched rubber specimens, Strain 42 (4) (2006) 299–304.

[19] Y. Guo, Z. Han, H. Guo, T. Wang, B. Liu, D. Wang, Numerical simulation damage analysis of pipe-cement-rock combination due to the underwater explosion, Engineering Failure Analysis 105 (2019) 584–596.

[20] A. Rajput, M. A. Iqbal, N. Gupta, Ballistic performances of concrete targets subjected to long projectile impact, Thin-Walled Structures 126 (2018) 171–181.

[21] T. Børvik, O. Hopperstad, T. Berstad, M. Langseth, A computational model of viscoplasticity and ductile damage for impact and penetration, European Journal of Mechanics-A/Solids 20 (5) (2001) 685–712.

[22] G.-M. Ren, H. Wu, Q. Fang, X.-Z. Kong, Parameters of holmquist–johnson–cook model for high-strength concrete-like materials under projectile impact, International Journal of Protective Structures 8 (3) (2017) 352–367.

[23] S. Hanchak, M. Forrestal, E. Young, J. Ehrgott, Perforation of concrete slabs with 48 mpa (7 ksi) and 140 mpa (20 ksi) unconfined compressive strengths, International Journal of Impact Engineering 12 (1) (1992) 1–7.

[24] J. Zukas, B. Gaskill, Ricochet of deforming projectiles from deforming plates, International journal of impact engineering 18 (6) (1996) 601–610.